ELSEVIER

Journal of Nuclear Materials 305 (2002) 70–76

journal of nuclear materials

www.elsevier.com/locate/jnucmat

Letter to the Editors

Creep strength of Zircaloy-4 cladding depending on applied stress and annealing temperature

Cheol Nam *, Byoung-Kwon Choi, Myung-Ho Lee, Yong-Hwan Jeong

Korea Atomic Energy Research Institute, 150 Dukjin-dong, Yusung, Daejon 305-500, South Korea

Received 28 January 2002; accepted 1 July 2002

Abstract

Tube creep tests were conducted on low tin Zircaloy-4 cladding with variations given in final annealing temperatures of 769–893 K, test temperatures of 613–673 K and applied hoop stresses of 90–195 MPa. The enhanced creep rates of low tin Zircaloy-4 by a factor of 2 compared with standard Zicaloy-4 were observed mainly due to reduced tin content. It was found that the creep parameters had a considerable stress dependency, that is, the activation energy and stress exponent decreased with stress increment. The plausible contribution of Coble creep to low-temperature-annealed Zircaloys at a lower stress range is discussed based on the determined creep parameters, microstructure and texture to explain the observed stress dependency.

PACS: 62.20.Hg; 81.40.Lm; 83.50.By; 91.60.Dc; 81.40.Ef

1. Introduction

Presently, low tin Zircaloy-4 is widely used as a fuel cladding material for pressurized water reactors. In this alloy, the amount of tin is controlled down to 1.3 wt% compared with 1.5 wt% of standard Zircaloy-4, in order to improve corrosion resistance of the cladding. Under normal operating conditions, the temperature of a cladding tube is in about 573–673 K. Early studies on circumferential creep of Zircaloy tube [1,2] in this temperature range showed that a large creep strain occurred in the stress-relieved material than in the recrystallized at low stresses, and vice versa at high stresses. The authors attributed the stress dependency to the difference in dislocation density. That is, as the applied stress increases a high dislocation density is required to maintain a steady-state creep rate, thus the stress-relieved structure having the high dislocation density exhibits the low creep strain at the high stress range.

However, only the dislocation density difference can hardly explain when it comes to axial creep. The axial creep strain of recrystallized Zircaloy-4 cladding was always larger than that of the stress-relieved even at the very low stress [1–3]. In addition, there are still considerable differences of opinion as to operating creep mechanism of α-phase zirconium alloys. At the low temperature range of 573–773 K, several deformation mechanisms such as climb-controlled dislocation creep [4,5], recovery creep [6,7], and grain boundary sliding (GBS) [8,9] have been suggested. At the temperatures higher than 773 K, Haper–Dorn creep [10] has been reported as well as diffusional creep [11–15] such as Nabarro–Herring creep and Coble creep. Even in the low temperature range, some authors [16,17] argued Coble creep as a plausible mechanism, especially at the low stress range.

The present work was undertaken to provide some insight into creep behaviors of low tin Zircaloy-4 cladding. Furthermore, an interpretation for the stress dependency of Zircaloy-4 creep with annealing condition is

* Corresponding author. Tel.: +82-42-868 8623; fax: +82-42-862 0432.

E-mail address: cnam@kaeri.re.kr (C. Nam).

0022-3115/02/$ - see front matter
PII: S0022-3115(02)00917-0

attempted based on the creep results and microstructure observations.

2. Experimental

The as-received Zircaloy-4 tube was manufactured from the same ingot and had the same production history. The tube had an outer diameter of 9.7 mm and a wall thickness of 0.63 mm. Its chemical composition is listed in Table 1. The as-received condition of the tube was cold-worked and stress-relieved at 769 K for 4 h. To obtain various annealing conditions, some samples were additionally annealed in a vacuum furnace for 4 h at the temperatures of 793, 853 and 893 K, respectively.

Nominal 15 cm long specimens were cut from the cladding tube and welded with a special end cap. These samples were assembled with a tube creep testing apparatus using Swagelok-type fittings. After attaining a specified test temperature in 3-zone furnace, the specimens were internally pressurized by argon gas. During the test, the specimen temperature was maintained within ± 3 K and the internal pressure was controlled in a negligible variation. The diametral change of the specimen was periodically measured with a digital micrometer at the three different axial locations of the specimen. Most of the tests were duplicated to reduce uncertainty. The hoop stress of a specimen, σ_θ, was predicted in accordance with the formula, $\sigma_\theta = 0.5P_iD_m/w$, where P_i is the internal pressure, D_m is the mid-wall diameter, and w is the thickness of the tube.

To preserve the dislocation structure, the specimens were cooled with the pressurized state. The transmission electron microscopy samples were prepared by chemically thinning the samples down to 80 μm, then jet-polished, to observe dislocations after creep deformation. For crystallographic texture measurement, the sample was cut into six pieces axially after cutting about 1.5 cm length of a tube, and the texture orientation was determined by X-ray diffraction in the circumferential-axial plane.

3. Results and discussion

3.1. Diametral creep of low tin Zircaloy-4

Fig. 1 shows the diametral creep curves of the as-received (annealed at 769 K × 4 h, hereafter referred to SR) and the recrystallized (annealed at 853 K × 4 h, hereafter referred to Rx) claddings. It is apparent from Fig. 1 that the SR exhibited larger hoop strains than the Rx when subjected to the low stresses, 90 and 120 MPa. On the contrary, the Rx showed the large creep strain at high stresses such as 135 and 150 MPa. This result manifests that there exists a transition stress from which the relative creep strength between the SR and the Rx is reversed. The transition stress observed in the present tests was around 120–135 MPa. Fig. 2 shows the effect of annealing temperature as a function of applied stress. In the low stress, the hoop creep strain decreased with annealing temperature increase, while the trend was reversed in the high stress condition. In the intermediate stress condition, minimum creep strain appeared in intermediately annealed claddings. All these behaviors of

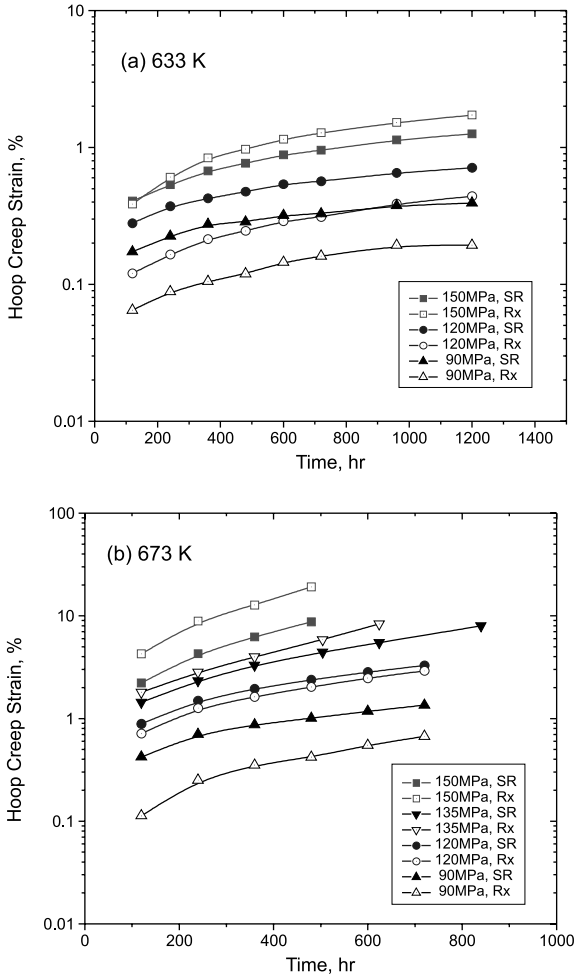

Fig. 1. Diametral creep curves for both the stress-relieved and the recrystallized Zircaloy-4 claddings at test temperatures of (a) 633 K and (b) 673 K.

Table 1
The chemical composition of Zircaloy-4 tube used in the experiment

Element	Sn	Fe	Cr	O	C	Si	Zr
wt%	1.27	0.23	0.12	0.13	0.016	0.010	Balance

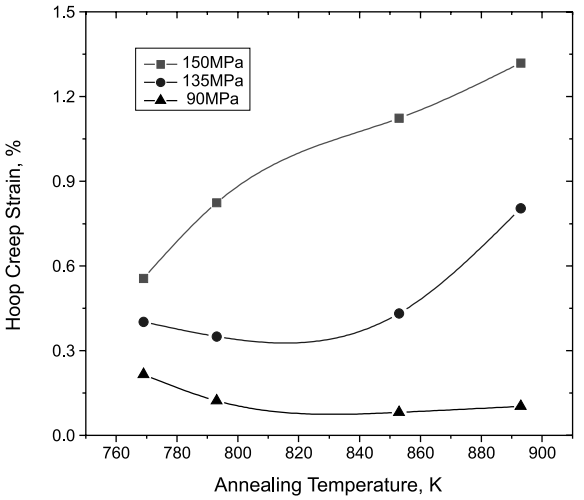

Fig. 2. Total creep strain versus annealing temperature tested at 613 K for 48 days.

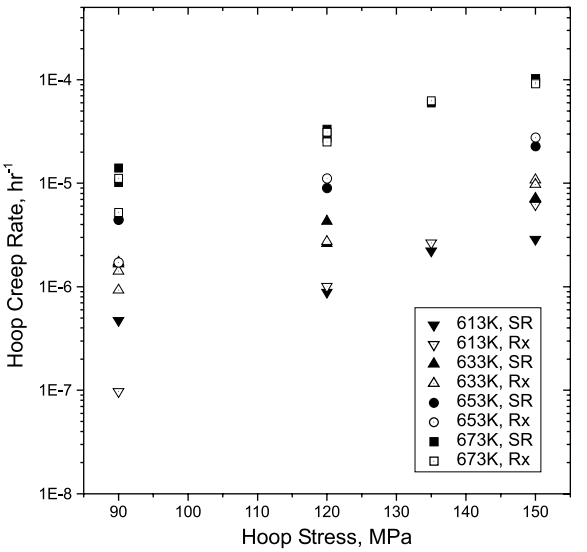

Fig. 3. Secondary creep rate versus hoop stress for low tin Zircaloy-4 tube.

the low tin Zircaloy-4 are well consistent with those of the standard Zircaloy-4 [1–3,18].

In determining a creep rate from a constant internal pressure test like the present experiment, attention should be paid since the actual stress increases as the tube is deformed. Because a negligible axial strain is expected in Zircaloy tube creep [19], the actual hoop stress increases due to the increment of diametral strain as well as the decrement of cladding thickness. Therefore, the relation between the true hoop stress and the diametral creep strain, $\sigma_\theta \approx \sigma_\theta^0(1+2\varepsilon_\theta)$, was considered in correcting the secondary creep rates. Fig. 3 represents the corrected secondary creep rates of the low tin Zircaloy-4 cladding against the applied stress. These creep rates are on average a factor of 2 higher than those of standard Zircaloy-4 tube (1.51% Sn) [20] regardless of the applied stress or test temperature. According to Ref. [21], 0.24% reduction in tin content (1.51–1.27%) could cause a factor of 2.58 increase in creep rate. Therefore, it can be inferred that the creep rate increase in low tin Zircaloy-4 is mainly attributed to the reduction of tin content.

Since the steady-state creep rate of Zircaloy-4 cladding exhibited high stress dependency, the sinh-type creep model has been widely used [20,22,23] in a practical point of creep rate modeling. However, the traditional way of describing creep rate is to use the Dorn-type model [24].

$$\dot{\varepsilon}_s = A\left(\frac{E}{T}\right)\left(\frac{\sigma}{E}\right)^n \exp\left(-\frac{Q_c}{RT}\right). \quad (1)$$

Here a and A are constants, n is stress exponent, Q_c is activation energy for creep, and E is Young's modulus, $1.148\times10^5 - 59.9T$ (K) in MPa [25]. The model constants, A, n and Q_c, were determined as 1.48×10^{18} K/MPa h, 3.47 and 193 kJ/mol for the SR, and 6.01×10^{22} K/MPa h, 5.37 and 185 kJ/mol for Rx, respectively. In general, if n is in the range of 4–7 and Q_c is similar to activation energy for self-diffusion, Q_{sd}, the creep mechanism is regarded as climb-controlled dislocation creep. However, the determined Q_c was lower than the Q_{sd} that is 259 kJ/mol in Zr–1.3% Sn alloy [26].

Saturated primary creep strain was determined from the extrapolation of secondary creep rate down to zero exposure time, and that is shown in Fig. 4. The primary creep strain increased both with the applied stress and the secondary creep rate. The Rx material showed more sensitive primary creep than the SR, depending on the applied stress and the secondary creep rate.

The activation energy variation with final annealing temperature was obtained by performing 'transient creep test' where the test temperature was suddenly increased during a test. As shown in Fig. 5, the large difference in creep activation energy between 90 and 195 MPa was found especially in low-temperature-annealed materials. Particularly at 90 MPa stressed SR tube, the activation energy for creep reduced markedly than that of the self-diffusion.

Fig. 6 shows double-log plot of the creep results in the Dorn-type model where the results of the steady-state tests and the transient tests are plotted altogether. In spite of different structural evolutions between the transient creep and the steady-state creep, both creep rates were well aligned in a trend line. Accordingly, the stress exponents for both the SR and Rx materials were determined depending on the range of applied stress (see Table 2). It is note worth that the stress exponent de-

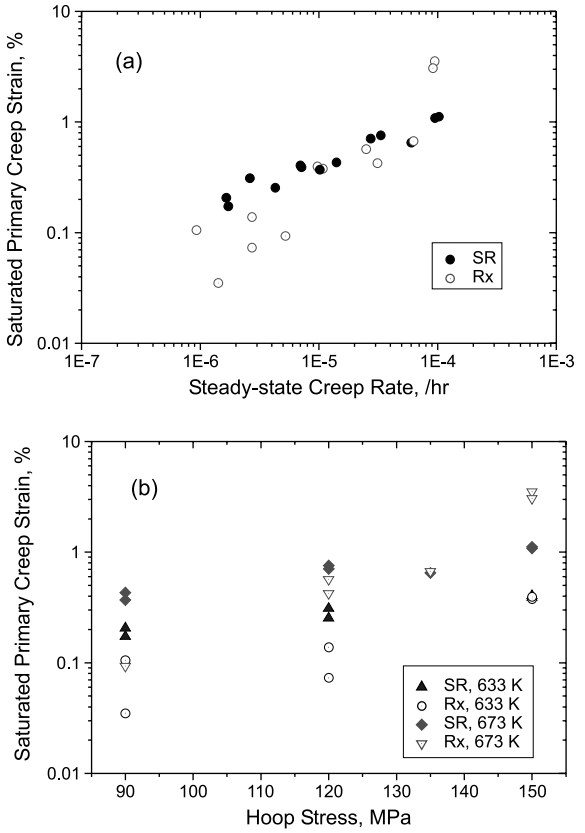

Fig. 4. Saturated primary creep strain as a function of (a) secondary creep rate and (b) hoop stress.

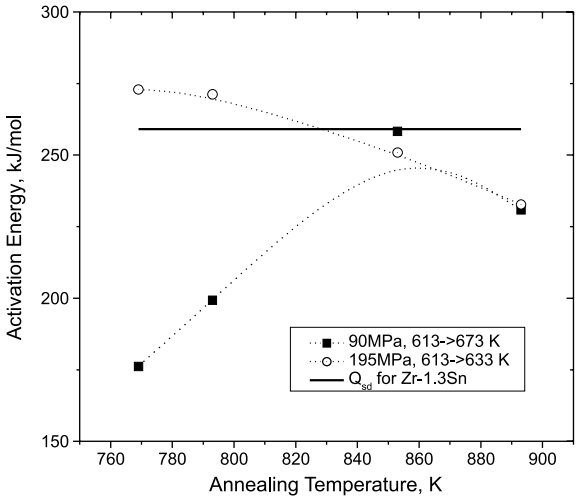

Fig. 5. Effect of stress level and annealing temperature on creep activation energy of Zircaloy-4 tube.

crease to 2.6 at the lower stress range in the SR tube that is less than the lower bound of climb-controlled creep

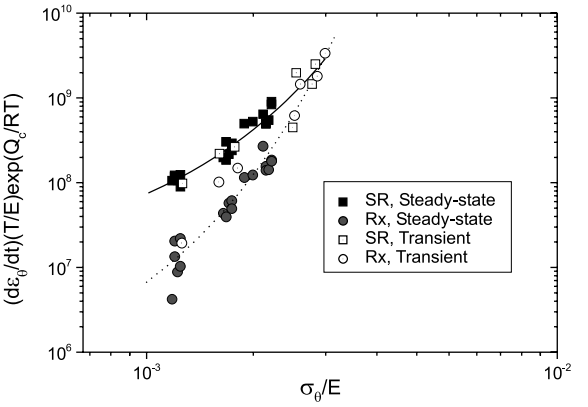

Fig. 6. Temperature compensated creep rate versus modulus compensated applied stress of Dorn-type creep model.

Table 2
Variation of stress exponent with the stress range in the stress-relieved and the recrystallized Zircaloy-4 material

	Stress range		
	90–120 MPa	120–150 MPa	150–195 MPa
SR	2.64	4.49	4.92
Rx	4.94	5.83	8.60

mechanism. The high stress exponents, especially in the Rx tube at the high stress range, may imply occurrence of power-law-breakdown so as to deform by dislocation glide-controlled mechanism.

3.2. Microstructure and texture

It is known that metallic zirconium deforms mainly by slip in $\langle a \rangle$ or $\langle a + c \rangle$ direction under high temperature and low stress conditions like creep deformation conditions. In the transmission electron microscopy study, since the transmitted beam was [0 0 0 1] zone axis, all the visible dislocations are $\langle a \rangle$ type or $\langle a + c \rangle$ type dislocations (see Fig. 7). The SR tube had an elongated and deformed grain structure, while the Rx tube had equiaxied grain structure with its diameter being about 7 μm. Small fractions of recrystallized grain were also observed in the SR tube, but its diameter was less than 2 μm. The samples crept at 90 MPa showed that almost all of the dislocations were individual ones. These were usually pinned or bowed at precipitations or intersected each other. It was observed some honey comb shape of dislocation networks as well as individual dislocations at 120 MPa stressed samples. In the 150 MPa crept samples, well-developed subgrains were observed usually in the vicinity of the grain boundary, while the dislocation substructure was not evident at 90 MPa stressed samples. Considering the fact that the development of

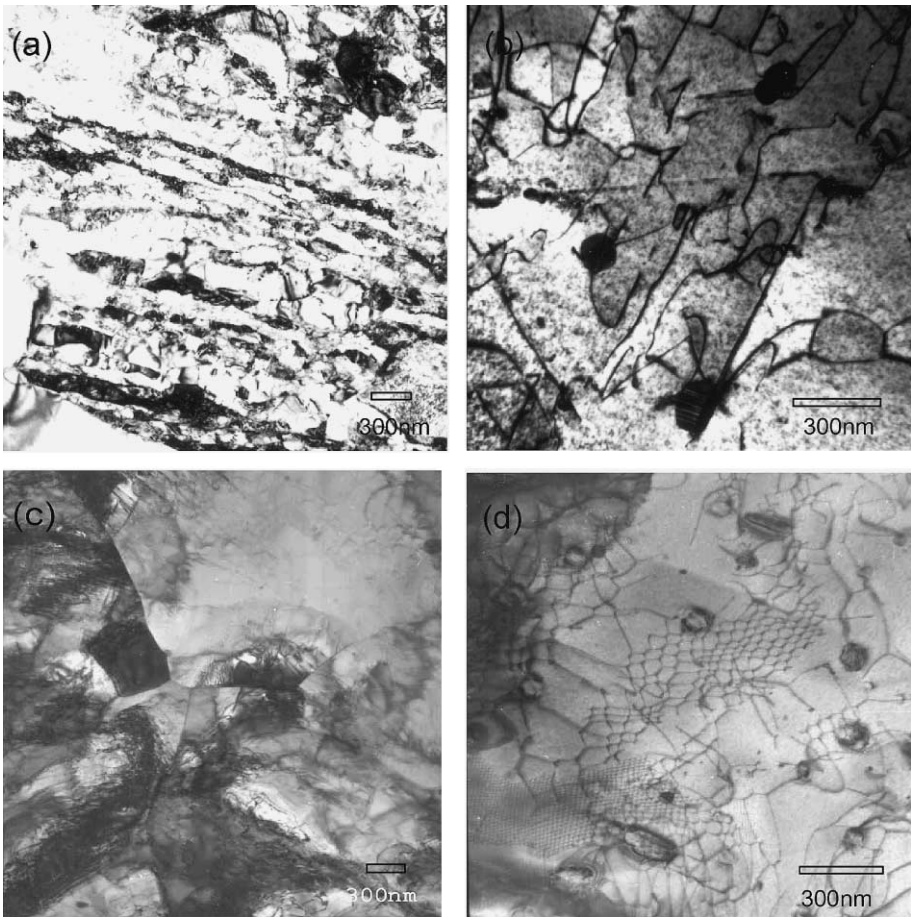

Fig. 7. Thin film TEM micrographs of Zircaloy-4 cladding crept at 400 °C: (a) SR tube at 90 MPa and 1.5% strain, (b) Rx tube at 90 MPa and 0.8% strain, (c) and (d) Rx tube at 150 MPa and 23% strain.

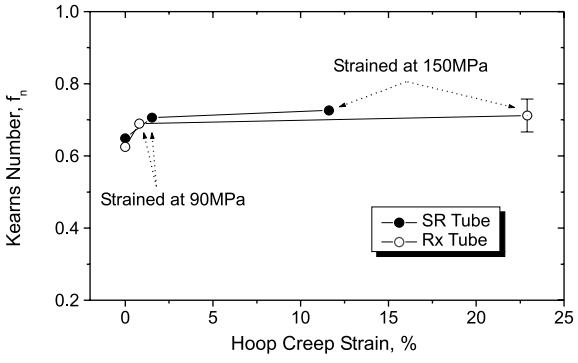

Fig. 8. Variation of Kearns texture number with creep strain.

dislocation substructure is a feature of climb-controlled creep mechanism, it can be inferred that the dislocation-climb controls Zircaloy creep at the high stresses but not at the low stresses.

No discernable shape change in pole figures after creep deformation was observed even after very high creep strain up to 23%, suggesting slip-dominated deformation. However, the Kearns texture number [27] was slightly increased as the creep strain increased (see Fig. 8). The reason for this is not clear now but some occurrence of twin might contribute to the increment of the texture number during creep deformation.

3.3. Creep mechanism at low stress range

It is obscure to explain the experimental observations of the Zircaloy creep only by the difference in the dislocation density because of the following reasons. According to the 'dislocation density' theory [1,2], if the same stress were applied to differently annealed materials, the dislocation density difference between the initial state and the steady state would disappear at the primary creep stage due to either by the recovery or the strain hardening, thus eventually the secondary creep

rate should approach to a constant rate independent of their final annealing condition. To be compatible with this, the primary creep strain of the SR tube should be a decreasing function as the stress increases. These are conflict with the test results shown in Figs. 3 and 4, respectively.

Considering the observed creep parameters of the SR tube with $n < 3$ and $Q_c < Q_{sd}$ at the low stress level, it can be envisaged either the activation of GBS or Coble creep because the phenomenological deformation rate for both deformation is usually expressed in the very similar formula

$$\dot{\varepsilon}_s = A\left(\frac{b}{d}\right)^3\left(\frac{\sigma}{E}\right)^n \exp\left(-\frac{Q_{gb}}{RT}\right). \quad (2)$$

Here, b is Berger's vector, d is grain size, and Q_{gb} is activation energy for grain boundary diffusion. In Eq. (2), $n = 1$ and $n = 2$ represent Coble creep and GBS, respectively. In Zircaloy, the value of Q_{gb} would be around 170 kJ/mol [12,28]. Although there are still a lot of discrepancies in n and Q_c for zirconium alloys in literature, at least it is evident that these values for stress-relieved Zircaloys tend to decrease to out of the range of climb-controlled creep as the applied stress decreases. For instance, at around 573–693 K test temperatures, the reported values of Q_c and n seem to be stress sensitive; 272 kJ/mol [23] at 78–314 MPa, 215 kJ/mol [20] at 51–126 MPa, and 113 kJ/mol and $n = 1.5$ [29] at 45–73 MPa. Commonly, GBS accompanies grain rotation during deformation, giving rise to a decrease in texture. From Fig. 8, however, no texture randomization was observed after creep deformation, suggesting a negligible deformation by GBS.

Therefore, it is plausible to assume that Coble creep becomes pronounced at the low stress level. Accordingly, the decreased creep strain with the increased annealing temperature at the low stress (see Fig. 2) is believed to be associated with its larger grain size. On the other hand, the predominance of dislocation-climb at the high stress would result in the decreased creep strain in the low-temperature-annealed materials due to their high dislocation densities. Thus the minimum creep strain appears at the intermediate annealing temperature under moderate stress level, where dislocation-climb and Coble creep compete. The larger creep strain of the stress-relieved than the recrystallized materials even at low stress range as low as 76 MPa in the axial creep testing of Zircaloys [1–3] can be rationalized by considering axially elongated grain structure of the stress-relieved claddings. The activation of Coble creep on this grain structure is hard to occur axially since a long diffusion distance is required to be deformed by Coble creep. Up to now, occurrence of Coble creep in the zirconium alloys has not been confirmed yet experimentally at temperatures less than 773 K, probably due to too much time consumption for a testing. However, extrapolation of Berstein's Coble creep model for Zircaloy-2 [12] down to the present test conditions gives a creep rate range of 1×10^{-5}–8×10^{-7} h^{-1} at the grain size range of 3–7 μm. These creep rates, especially at small grain size, are comparable to the present creep rates at low stress level, which also supports the contribution of Coble creep.

4. Conclusions

No significant differences of the creep behaviors of low tin Zircaloy-4 tube were observed depending on the variations in stress and final annealing when compared with standard Zircaloy-4 cladding in literature, except for the fact that the creep rates of the former were higher than those of the latter by a factor of 2. From the investigation on creep parameters, microstructure and texture, it is inferred that Coble creep seems to occur in parallel with climb-controlled dislocation creep and it becomes prominent at lower stresses and smaller grain sizes.

Acknowledgements

The authors acknowledge that this study is carried out under the Nuclear R&D Program planned by the Korean Ministry of Science and Technology.

References

[1] K. Kallstrom, T. Andersson, A. Hofvenstam, ASTM STP 551 (1974) 160.
[2] R.J. Beauregard, G.S. Clevinger, K.L. Murty, Proceedings of the 4th International Conference SMiRT, San Francisco, CA, 1977, C3/5.
[3] H. Stehle, E. Steinberg, E. Tenckhoff, ASTM STP 633 (1977) 486.
[4] K.L. Murty, G.S. Clevinger, T.P. Papazoglou, Proceedings of the 4th International Conference SMiRT, San Francisco, CA, 1977, C3/4.
[5] Y.S. Kim, J. Nucl. Mater. 250 (1997) 164.
[6] M. Pahutova, J. Cadek, J. Nucl. Mater. 61 (1976) 285.
[7] W.R. Thorpe, I.O. Smith, J. Nucl. Mater. 75 (1978) 209.
[8] F.H. Huang, G.P. Gabol, S.G. McDonald, Che-Yu Li, J. Nucl. Mater. 79 (1979) 214.
[9] K.L. Murty, B.V. Tanikella, J.C. Earthman, Acta Metall. Mater. 42 (11) (1994) 3653.
[10] J. Novotny, J. Fiala, J. Cadek, Acta Metall. 33 (5) (1985) 905.
[11] R.B. Jones, J. Nucl. Mater. 19 (1966) 204.
[12] I.M. Bernstein, Trans. Metall. Soc. AIME 239 (1967) 1518.
[13] A.J. Ardell, O.D. Sherby, Trans. Metall. Soc. AIME 239 (1967) 1547.

[14] N. Prasad, G. Malakondaiah, P. Rama Rao, Scrip. Metall. 26 (1992) 541.
[15] K.L. Murty, J. Ravi, Wiratmo, Nucl. Eng. Design 156 (1995) 359.
[16] M. Pahutova, J. Cadek, V. Cerny, J. Nucl. Mater. 68 (1977) 111.
[17] E. Kohn, M.G. Wright, J. Nucl. Mater. 98 (1981) 247.
[18] J.M. Frenkel, M. Weisz, ASTM STP 551 (1974) 140.
[19] K.L. Murty, B.L. Adams, Mater. Sci. Eng. 70 (1985) 169.
[20] M. Mayuzumi, T. Onch, J. Nucl. Mat. 171 (1990) 381.
[21] C. Nam, K.H. Kim, M.H. Lee, Y.H. Jeong, J. Kor. Nucl. Soc. 32 (2000) 372.
[22] M. Limback, T. Andersson, ASTM STP 1295 (1996) 448.
[23] Y. Matsuo, J. Nucl. Sci. Technol. 24 (1987) 111.
[24] J.E. Bird, A.K. Mukherjee, J.E. Dorn, Quantitative Relations between Properties and Microstructure, Israel University, 1969, p. 225.
[25] USNRC, TREE-NUREG-1005, 1976.
[26] V.S. Lyashenko, V.N. Bykor, L.V. Pavlinov, Phys. Met. Metall. 8 (1960) 40.
[27] J.J. Kearns, Thermal Expansion and Preferred Orientation in Zircaloy, Westinghouse Co. Report, WAPD-YM-472, 1965.
[28] N. Prasad, G. Malakondaiah, K. Muraleedharan, P. Rama Rao, J. Nucl. Mater. 158 (1988) 30.
[29] H. Maki, T. Hara, J. Nucl. Sci. Technol. 12 (1) (1975) 43.